J. Plasma Phys. (2022), *vol*. 88, 175880302
Published by Cambridge University Press
doi:10.1017/S0022377822000447

LETTER

High-energy proton beam acceleration driven by an intense ultrarelativistic electron beam in plasma

Xiangyang Liu[1,2], Houchen Fan[1], Junfan Qu[1], Peng Liu[1], Guangyi Zhao[1], Liru Yin[1], Xiaofeng Li[3,4], Qin Yu[5], Linwen Zhang[2] and Qing Kong[1,†]

[1]Key Laboratory of Nuclear Physics and Ion-beam Application (MOE), Institute of Modern Physics, Department of Nuclear Science and Technology, Fudan University, Shanghai 200433, PR China

[2]Institute of Fluid Physics, CAEP, Mianyang 621900, PR China

[3]Key Laboratory for Laser Plasmas (MoE), School of Physics and Astronomy, Shanghai Jiao Tong University, Shanghai 200240, PR China

[4]Collaborative Innovation Center of IFSA (CICIFSA), Shanghai Jiao Tong University, Shanghai 200240, PR China

[5]State Key Laboratory of High Field Laser Physics and CAS Center for Excellence in Ultra-intense Laser Science, Shanghai Institute of Optics and Fine Mechanics, Chinese Academy of Sciences, Shanghai 201800, PR China

(Received 11 January 2022; revised 29 April 2022; accepted 3 May 2022)

We report a generation of energetic protons by the interaction of a high-energy electron driving beam with an underdense plasma slab. After an interaction period of approximately 4000 fs, a proton beam with maximum energy greater than 250 MeV can be achieved by applying a driving beam with energy 1.0 GeV to a 200 μm plasma slab. Our two-dimensional particle-in-cell simulations also show that the proton acceleration process can be divided into two stages. In the first stage, a strong positive longitudinal electric field appears near the rear boundary of the plasma slab after the driving beam has passed through it. This acceleration process is similar to the target normal sheath acceleration scheme by the interaction between intense pulsed laser with overdense plasma targets. In the second stage, the accelerated protons experience a long-range acceleration process with a two-stream instability between the high-energy driving beam and the proton beam. Further analyses show that this accelerated proton beam is equipped with the property of good collimation and high energy. This scheme presents a new way for proton or ion acceleration on some special occasions.

Key words: intense particle beams, plasma applications

In recent years, charged particles acceleration by plasma wakefields has attracted great interest. One of the most attractive advantages of the plasma wakefield is the large acceleration gradient. For plasma with a density of 10^{18} cm^{-3}, the typical amplitude of

† Email address for correspondence: qkong@fudan.edu.cn

acceleration field E_0 can reach approximately 100 GV m^{-1} according to the wave breaking limit (Dawson 1959; Lotov 2010), making it possible to accelerate charged particles to relativistic energy within an ultrashort length. When an intense pulsed laser or a relativistic particle beam interacts with plasma, a plasma wakefield can be excited and used to accelerate charged particles, known as LWFA (Laser wakefield accelerator) (Tajima & Dawson 1979; Pukhov & Meyer ter Vehn 2002) or PWFA (Plasma wakefield accelerator) (Chen *et al.* 1985), respectively. In the past few decades, both the LWFA and PWFA have been widely studied in electron acceleration (Pukhov, Sheng & Meyer ter Vehn 1999; Blumenfeld *et al.* 2007; Wang *et al.* 2013; Litos *et al.* 2016; Gonsalves *et al.* 2019; Rosmej *et al.* 2020), and much progress has already been made. At the same time, the interaction of pulsed laser with high density plasma has also been used to accelerate ions (Qiao *et al.* 2009; Liu *et al.* 2020). These energetic ions have wide applications, such as astrophysics (Remington *et al.* 2000), proton radiography (King *et al.* 1999), tumour therapy (Bulanov & Khoroshkov 2002) and fast ignition (Roth *et al.* 2001). At present, many ion acceleration schemes based on pulsed laser–plasma interaction have been developed, such as target normal sheath acceleration (TNSA) (Maksimchuk *et al.* 2000; Snavely *et al.* 2000; Wilks *et al.* 2001), radiation-pressure acceleration (RPA) (Esirkepov *et al.* 2004; Macchi *et al.* 2005; Robinson *et al.* 2008; Yan *et al.* 2008; Macchi, Veghini & Pegoraro 2009; Qiao *et al.* 2009; Shen *et al.* 2017), shockwave acceleration (Fiuza *et al.* 2012; Zhang *et al.* 2016), peeler acceleration (Shen, Pukhov & Qiao 2021), cascaded acceleration (Gonoskov *et al.* 2009; He *et al.* 2019) and the breakout afterburner scheme (Yin *et al.* 2006, 2007).

Compared with LWFA, using the PWFA scheme to accelerate electrons can reduce the influence caused by phase slippage, so that it is easier to achieve stable long-range acceleration (Shin 2014). At the same time, it is possible to take advantage of the high-energy electron beams generated by the traditional accelerators that have already been built (Blumenfeld *et al.* 2007; Litos *et al.* 2014, 2016) around the world. However, the investigations on the use of PWFA to accelerate ions are relatively few, to date. In this paper, we propose a new proton acceleration scheme by the interaction of a relativistic electron beam with an underdense plasma slab. As our two-dimensional (2-D) particle-in-cell (PIC) simulations show, when the electron driving beam travels into the middle of the plasma slab, a wakefield can be excited, as in the well known bubble regime. After the driving beam has propagated through the plasma region, a bunch of proton beams can be pulled out following the driving beam, similar to the TNSA scheme in the laser-driven proton acceleration. Then these protons can be accelerated continuously to energies up to several hundreds of MeV in vacuum. In the absence of superpulsed lasers, it would make sense to obtain high-energy protons using the mechanism proposed in this paper. In the following, the physics behind this acceleration scheme is discussed in detail.

In general, when a high-power pulsed laser beam propagates into a plasma, it can excite a linear or nonlinear wakefield, depending on the intensity of the laser (Lu *et al.* 2005). The situation is similar when the driving beam is a relativistic electron beam. When a relativistic electron beam with low charge value propagates into an underdense plasma, a linear wakefield will be formed. If the driving beam has a high charge value and high density, the linear wakefield will turn into a nonlinear wakefield, and this case is also called the bubble region (Lu *et al.* 2006). As a typical case in our 2-D simulation, a bi-Gaussian driving beam is incident from the left-hand of the simulation box along the x direction. In the case of using the EPOCH 'injector' module, the density profile of the driving beam can be described as

$$n_b = n_{b0} \exp\left[-\frac{r^2}{2\sigma_r^2} - \frac{(t-3\sigma_{t0})^2}{2\sigma_{t0}^2}\right], \tag{0.1}$$

https://doi.org/10.1017/S0022377822000447 Published online by Cambridge University Press

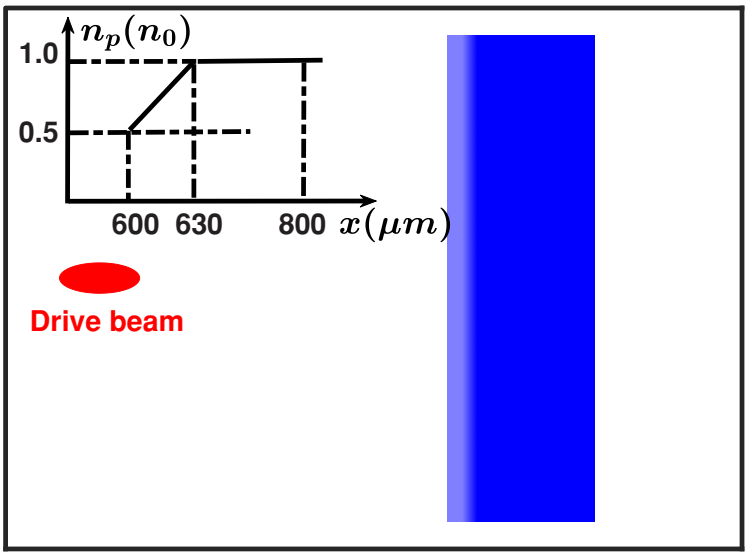

FIGURE 1. Schematic diagram of the 2-D PIC simulation box and the plasma density profiles n_p. The driver beam is represented by a red ellipse.

where $\sigma_{t0} = 80.0\ \mu\text{m}\ c^{-1}$; $\sigma_r = 4.22/k_p = 10.0\ \mu\text{m}$; $k_p = \sqrt{n_0 e^2/(\varepsilon_0 m_e c^2)}$ is the plasma wavenumber; $n_0 = 5.0 \times 10^{18}\ \text{cm}^{-3}$ is the plasma density; e, m_e and c are the charge value of a unit charge, the rest mass of an electron and the speed of light, respectively. The longitudinal distribution of the driving beam is controlled by the time parameters t and σ_{t0}. The initial energy of the driving beam is 1.0 GeV per particle, and its peak density is $n_{b0} = 4.0 \times 10^{18}\ \text{cm}^{-3}$. The charge value of the driving beam is approximately 3.19 nC μm^{-1}. The 2-D simulations were carried out using the PIC code EPOCH (Arber *et al.* 2015). The 'simple outflow' boundary conditions are used on the simulation box front and back boundary, and the lateral boundary conditions are 'open'. The simulation box is a rectangular area of 1500 μm $\times$ 800 μm which has 7500 grids in the x direction and 4000 grids in the y directions, and four superparticles per cell for each particle species. The plasma slab is composed of electrons and protons ranging from $x = 600$ μm to $x = 800$ μm, and it is composed of a 30 μm up-ramp region and a 170 μm platform region. In the density up-ramp transitional region ($x = 600$–630 μm), plasma density increases linearly from $0.5n_0$ to n_0; in the platform region ($x = 630$–800 μm), plasma density keeps constant n_0. The schematic diagram of the PIC simulation box is shown in figure 1. As is shown in this figure, the relativistic electron beam is represented by a red ellipse.

To clearly describe the interaction process of the relativistic electron beam with plasma, we present the electron and proton number density of the typical 2-D simulation case at different specific moments (t = 3100 fs, 4400 fs and 6800 fs) in figure 2, where figure 2(*a–c*) show the electron number density and figure 2(*d–f*) show the proton number density. The number density value is represented by the colourbar and has been normalized with n_0. As mentioned above, since the driving beam has a high charge value and energy, when the driving beam moves into the plasma slab, the background electrons are pushed away laterally by the expelling force of the driving beam. Therefore, an electron bubble is formed as shown in figure 2(*a*). At this time, figure 2(*d*) shows that the background protons are also disturbed, but these protons do not have a large displacement because the mass of a proton is much larger than that of an electron. If the length of the plasma target is long

https://doi.org/10.1017/S0022377822000447 Published online by Cambridge University Press

enough, the bubble will move following the driving beam while the driving beam will lose energy continuously. This scheme may enter a process of electron acceleration in the bubble. However, if the plasma length is limited to a reasonably small value, such as the bubble length, the driving beam will quickly pass through the plasma region. As a result, the plasma bubble cannot remain closed for a long time. Since the plasma density is higher than the driving beam density, the background electrons can be quickly pulled back by the positively charged ions. Therefore, the plasma bubble is relatively small, as expected. In figures 2(*b*) and 2(*e*), one can see that the driving beam has passed through the plasma slab at $t = 4400$ fs, a low-density channel-like structure is formed in the middle of the plasma region, and a bunch of protons has rushed out of the right-hand boundary of the plasma slab into the vacuum at the same time. It should be noted that the profile of the driving beam has evolved from a Gaussian shape to a fish-like shape which has a fishtail-like structure at its rear. After that, the driving beam leaves the plasma with a velocity very close to the speed of light in a vacuum, just as shown in figure 2(*c*). Meanwhile, the background plasma electrons at 6800 fs, which do not have enough energy to catch up with the driving beam and the high-energy proton beam, stay in the region around the plasma slab and form an electron cloud. In figure 2(*f*), the accelerated protons have also moved farther from the right-hand boundary of the plasma region and form a proton bunch with good collimation.

To give a more detailed study on the proton acceleration mechanism, we plot the longitudinal electric field on the central axis $r = 0$ (represented by the blue line) and the driving beam (represented by a purple block) at different times in figure 3. Dotted black lines indicate the initial left-hand and right-hand boundaries of the plasma slab. Apart from this, protons with energy greater than 50 MeV at 7500 fs are tracked and drawn in these diagrams, and the unit of the colourbar representing the energy of the tracked protons is MeV. At 3100 fs, one can see that the longitudinal electric field E_x in figure 3(*a*) is similar to the wakefield in a plasma bubble, and the peak value of the positive field is approximately 5 GV cm^{-1}. All traced protons are located near the right-hand boundary of the plasma slab, and their energy is not greater than 1.0 MeV. This means that the protons at this time have not been accelerated yet. However, as the main part of the driving beam rushes out of the right-hand boundary of the plasma, the positive electric field peak value quickly increased to around 15.0 GV cm^{-1}, as shown in figure 3(*b*). This phenomenon is because the charge of the driving beam is concentrated in a small area and the driving beam is very close to the positively charged ion area in plasma. At this moment, a strong charge separation field is formed. The positive field coming from the driving beam superposition with the charge separation field forms an enhanced acceleration field which can accelerate the traced protons violently. At 3700 fs, some of the traced protons have been accelerated to approximately 20 MeV. At 4400 fs, the maximum energy of these protons has exceeded 100 MeV, as shown in figure 3(*c*). From this figure, it can be seen that the amplitude of the positive longitudinal field has decreased but is still greater than 6 GV cm^{-1}. The strong longitudinal field can accelerate protons quickly, just like the field in the TNSA scheme. Compared with the TNSA scheme driven by a pulsed laser, the electron driving beam has small energy spread, good collimation and higher energy, so it is expected to obtain a higher quality accelerated proton beam in this scheme. The following analyses show that the accelerated protons do have good collimation and high energy. After the driving beam has rushed out from the plasma slab completely, the rear of the driving beam evolves into a fishtail shape, and there is an electric field peak appearing at the place where the tail of the driving beam and the head of the traced proton beam overlap. It is worth mentioning that the fishtail structure forms a flat distribution of longitudinal electric

https://doi.org/10.1017/S0022377822000447 Published online by Cambridge University Press

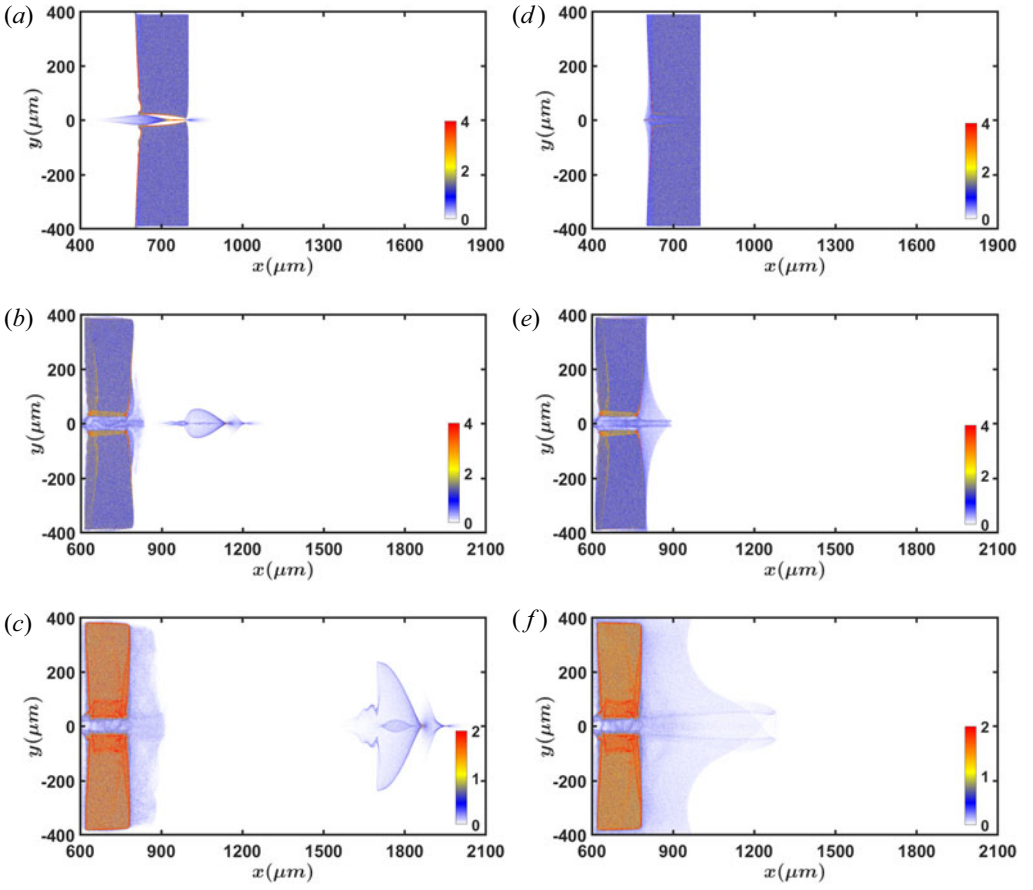

FIGURE 2. Panels (*a–c*) show the number density of the background electrons and the driving beam at $t = 3100$ fs, 4400 fs and 6800 fs, respectively. Panels (*d–f*) are the number density of the background protons at $t = 3100$ fs, 4400 fs and 6800 fs, respectively. The number density value is displayed by the colourbar and has been normalized with the background plasma density n_0.

field along the transverse direction, which can also lead to better collimation compared with that of the TNSA scheme.

Thereafter, the proton beam and driving beam form a two-stream instability structure, and the protons undergo a long-range acceleration process. As shown in figure 3(*d*), the peak of E_x has decreased to 3.4 GV cm^{-1} at 6800 fs, but the longitudinal distribution length of the positive field has also become longer, and the proton beam is still located in an acceleration phase. At the position of the driving beam, there is a longitudinal electric field of approximately 2.4 GV cm^{-1}. There are two main sources of this longitudinal electric field, one of which is the lateral movement of the driving beam electrons. It is impossible for any energy electron beam in vacuum to remain collimated and so it must expand laterally. This will generate an E_y. The second part is the charge separation field between the driving beam and the accelerated protons, although it is much smaller than before. The superposition of these two electric fields results in the 2.4 GV cm^{-1} longitudinal electric field at the position of the driving beam. Because the speed of protons is smaller than that of the driving beam, the accelerated protons will gradually slip backward relative to the driving beam. As the longitudinal field E_x on the central axis becomes weaker, the

https://doi.org/10.1017/S0022377822000447 Published online by Cambridge University Press

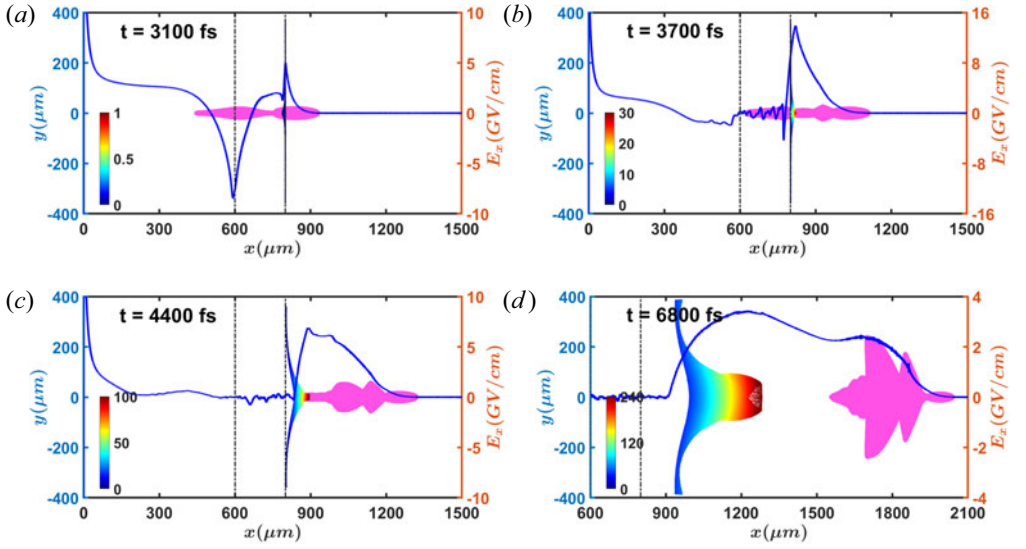

FIGURE 3. The longitudinal electric field along $y = 0$ (represented by the blue lines) and the electron driver beam (represented by a purple block) at 3100 fs (*a*), 3700 fs (*b*), 4400 fs (*c*) and 6800 fs (*d*), respectively. At the same time, the space–energy distribution of the protons with energy greater than 50 MeV at 7500 fs are also drawn in these diagrams, and the unit of the colourbar is MeV.

energy increase of the accelerated protons will become slow. This long-range acceleration process can last a long time until the distance between the proton beam and the driving beam is too large to maintain a strong acceleration field for protons or the driving beam collapses. Figure 3(*d*) also shows that the maximum energy of the traced protons has exceeded 200 MeV.

In order to analyse the beam quality of the accelerated proton beam in our scheme, we plot the space–energy distribution of protons emitted from the plasma slab, the energy spectrum, and the angular spectrum of protons with energy greater than 100 MeV at 7500 fs in figure 4. The colourmap in figure 4(*a*) shows the proton energy value, and the units of colourbar are MeV. From this figure, it is easy to find that most of the protons with energy greater than 100 MeV are distributed in $x = 1100$–1500 μm, and the protons with the maximum energy are distributed in the head part of the accelerated proton beam. Figure 4(*b*) presents the energy spectrum of the protons with energy greater than 100 MeV at $t = 7500$ fs. It can be found that the maximum proton energy E_{max} is close to 300 MeV. The angular spectrum of the accelerated protons is shown in figure 4(*c*). From this figure, one can find that the divergence angle of the protons has two peaks at $\theta = 9^\circ$ and $\theta = -9^\circ$. The normalized emittance of the protons with energy greater than 100.0 MeV at $t = 7500$ fs is $\varepsilon_{p,rms} = 0.46\pi$ mm mrad, calculated by Floettmann (2003),

$$\varepsilon_{p,rms} = \frac{1}{m_p c}\sqrt{\langle y^2\rangle\langle p_y^2\rangle - \langle y p_y\rangle^2}, \tag{0.2}$$

where m_p is the rest mass of the proton. This result means that this proton beam has good collimation. What is more, the charge value of the protons with energy greater than 100.0 MeV is approximately 0.46 nC μm^{-1}. As mentioned above, the proton acceleration process can be divided into two stages: the TNSA-like acceleration stage and the

https://doi.org/10.1017/S0022377822000447 Published online by Cambridge University Press

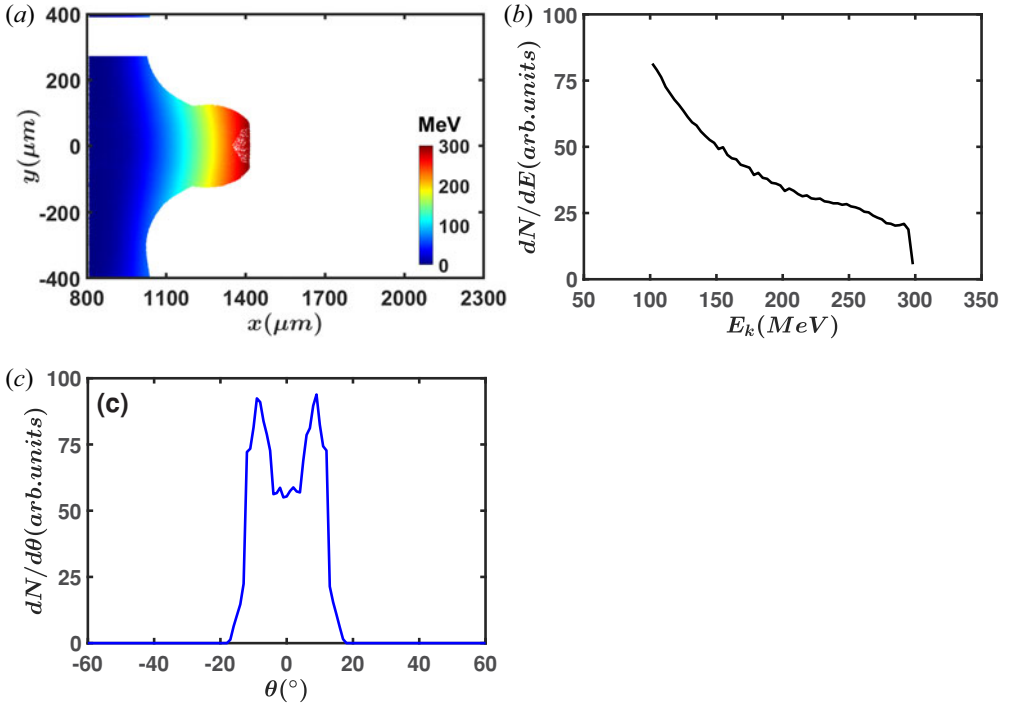

FIGURE 4. The analyses of the accelerated proton beam. Panel (*a*) shows the space–energy distribution of protons at $t = 7500$ fs. The unit of the colourbar is MeV. Panels (*b*) and (*c*) are the energy spectrum and angular spectrum of protons with energy greater than 100 MeV at $t = 7500$ fs, respectively.

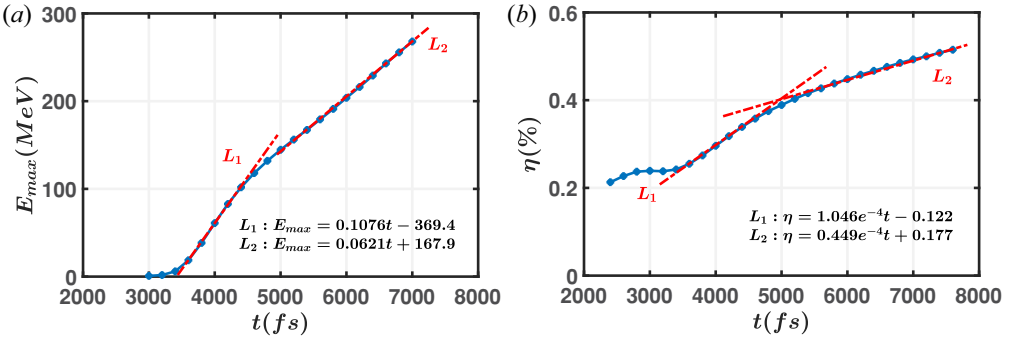

FIGURE 5. (*a*) The temporal evolution of the maximum energy E_{max} of the accelerated protons. (*b*) The temporal evolution of the energy loss percentage η of the driving beam. The red dotted lines L_1 and L_2 represent the linear fit to the data in (*a*) and (*b*).

long-range acceleration stage, which are further confirmed by the following analyses in figure 5. The temporal evolution of the maximum energy of the accelerated protons E_{max} is shown in figure 5(*a*). Before 3200 fs, the background protons do not gain energy. From 3200 fs, some protons start to be accelerated, especially from 3600 fs to 4600 fs, E_{max} increases from 18.6 MeV to 118.0 MeV quickly. Combined with the discussion above, this stage belongs to a scheme of TNSA-like acceleration. In 5000 fs–7000 fs, the growth

https://doi.org/10.1017/S0022377822000447 Published online by Cambridge University Press

of E_{max} slowed down, and this is consistent with the long-range acceleration process. After 2000 fs acceleration, E_{max} is still able to increase from approximately 120 MeV to 268 MeV. The two red dotted lines L_1 and L_2 in figure 5(*a*) represent the linear fit of E_{max} in these two stages. It can be seen that the energy increase rate of the first stage is approximately two times that of the second stage. In figure 5(*b*), the evolution of energy loss percentage η over time is presented, and η is defined as the lost energy divided by the initial total energy of the driving beam. This figure also indicates that η is different in two acceleration stages. The two red dotted lines L_1 and L_2 in figure 5(*b*) show the linear fit of η in two stages. The slopes of L_1 and L_2 indicate that the energy lost speed in the first stage is larger than twice that of the second stage, inferring that when the driving beam just rushes out of the plasma boundary energy can be transferred rapidly from the driving beam to the background protons. In the second acceleration stage, the energy conversion rate starts to slow down. From figure 5(*b*), one can see the remaining energy of the driving beam is approximately 50 % at 7000 fs. In addition, it is found that 14.2 % of the energy of the driving beam is converted into the kinetic energy of the accelerated proton beam at 7000 fs. Thereafter, the acceleration field weakens with the increase of distance between two streams and this is the most critical reason in the termination of proton acceleration. From the above results it can be seen that the energy conversion efficiency from the driving beam to protons still has great potential for improvement; to find some ideas to improve the energy transfer ratio requires further investigations. Besides, it should be noted that the proton acceleration mechanism proposed in this paper relies on a driving beam generation method with large charge value. Perhaps an intense laser interacting with a near-critical plasma density could produce an electron beam with such a large charge.

In summary, we proposed a proton acceleration scheme through the interaction of a high-energy electron beam with an underdense plasma slab. Our simulations show that the protons can be accelerated by a TNSA-like process, followed by a long-range acceleration mechanism. The accelerated protons can obtain energy up to approximately 250 MeV within a period of around 4000 fs acceleration by an electron driving beam with an energy of 1.0 GeV per particle. Compared with protons accelerated by the TNSA scheme, the proton beam accelerated by the electron driving beam has good beam quality, high energy and good collimation. The proton acceleration scheme proposed in this paper provides a new way to generate high energy protons or ions and may be used for nuclear fusion and material treatment.

Acknowledgements

Editor V. Malka thanks the referees for their advice in evaluating this article.

Declaration of interest

The authors report no conflict of interest.

Funding

We acknowledge the financial support from the National Natural Science Foundation of China (no. 11775056 and no. 11804348).

REFERENCES

Arber, T.D., Bennett, K., Brady, C.S., Lawrence-Douglas, A., Ramsay, M.G., Sircombe, N.J., Gillies, P., Evans, R.G., Schmitz, H., Bell, A.R., *et al.* 2015 Contemporary particle-in-cell approach to laser-plasma modelling. *Plasma Phys. Control. Fusion* **57** (11), 113001.

BLUMENFELD, I., CLAYTON, C.E., DECKER, F.-J., HOGAN, M.J., HUANG, C., ISCHEBECK, R., IVERSON, R., JOSHI, C., KATSOULEAS, T., KIRBY, N., *et al.* 2007 Energy doubling of 42 GeV electrons in a metre-scale plasma wakefield accelerator. *Nature* **445** (7129), 741–744.

BULANOV, S.V. & KHOROSHKOV, V.S. 2002 Feasibility of using laser ion accelerators in proton therapy. *Plasma Phys. Rep*. **28** (5), 453–456.

CHEN, P., DAWSON, J.M., HUFF, R.W. & KATSOULEAS, T. 1985 Acceleration of electrons by the interaction of a bunched electron beam with a plasma. *Phys. Rev. Lett*. **54** (7), 693–696.

DAWSON, J.M. 1959 Nonlinear electron oscillations in a cold plasma. *Phys. Rev*. **113** (2), 383–387.

ESIRKEPOV, T., BORGHESI, M., BULANOV, S.V., MOUROU, G. & TAJIMA, T. 2004 Highly efficient relativistic-ion generation in the laser-piston regime. *Phys. Rev. Lett*. **92** (17), 175003.

FIUZA, F., STOCKEM, A., BOELLA, E., FONSECA, R.A., SILVA, L.O., HABERBERGER, D., TOCHITSKY, S., GONG, C., MORI, W.B. & JOSHI, C. 2012 Laser-driven shock acceleration of monoenergetic ion beams. *Phys. Rev. Lett*. **109** (21), 215001.

FLOETTMANN, K. 2003 Some basic features of the beam emittance. *Phys. Rev. Spec. Top. - Accel. Beams* **6** (3), 034202.

GONOSKOV, A.A., KORZHIMANOV, A.V., EREMIN, V.I., KIM, A.V. & SERGEEV, A.M. 2009 Multicascade proton acceleration by a superintense laser pulse in the regime of relativistically induced slab transparency. *Phys. Rev. Lett*. **102** (18), 184801.

GONSALVES, A.J., NAKAMURA, K., DANIELS, J., BENEDETTI, C., PIERONEK, C., DE RAADT, T.C.H., STEINKE, S., BIN, J.H., BULANOV, S.S., VAN TILBORG, J., *et al.* 2019 Petawatt laser guiding and electron beam acceleration to 8 GeV in a laser-heated capillary discharge waveguide. *Phys. Rev. Lett*. **122** (8), 084801.

HE, H., QIAO, B., SHEN, X.F., YAO, W.P., YAO, Y.L., ZHOU, C.T., HE, X.T., ZHU, S.P., PEI, W.B. & FU, S.Z. 2019 All-optical cascaded ion acceleration in segmented tubes driven by multiple independent laser pulses. *Plasma Phys. Control. Fusion* **61** (11), 115005.

KING, N.S.P., ABLES, E., ADAMS, K., ALRICK, K.R., AMANN, J.F., BALZAR, S., BARNES JR., P.D., CROW, M.L., CUSHING, S.B., EDDLEMAN, J.C., *et al.* 1999 An 800-MeV proton radiography facility for dynamic experiments. *Nucl. Instrum. Meth. Phys. Res. Sec.* A*: Accel. Spectrom. Detect. Assoc. Equip*. **424** (1), 84–91.

LITOS, M., ADLI, E., AN, W., CLARKE, C.I., CLAYTON, C.E., CORDE, S., DELAHAYE, J.P., ENGLAND, R.J., FISHER, A.S., FREDERICO, J., *et al.* 2014 High-efficiency acceleration of an electron beam in a plasma wakefield accelerator. *Nature* **515** (7525), 92–95.

LITOS, M., ADLI, E., ALLEN, J.M., AN, W., CLARKE, C.I., CORDE, S., CLAYTON, C.E., FREDERICO, J., GESSNER, S.J., GREEN, S.Z., *et al.* 2016 9 GeV energy gain in a beam-driven plasma wakefield accelerator. *Plasma Phys. Control. Fusion* **58** (3), 034017.

LIU, P., QU, J., LIU, X., LI, X., CAI, L., TANG, J. & KONG, Q. 2020 Beam quality improvement in the later stage of radiation pressure acceleration. *Phys. Rev. Accel. Beams* **23** (1), 011303.

LOTOV, K.V. 2010 Simulation of proton driven plasma wakefield acceleration. *Phys. Rev. Spec. Top. - Accel. Beams* **13** (4), 041301.

LU, W., HUANG, C., ZHOU, M.M., MORI, W.B. & KATSOULEAS, T. 2005 Limits of linear plasma wakefield theory for electron or positron beams. *Phys. Plasmas* **12** (6), 063101.

LU, W., HUANG, C., ZHOU, M., TZOUFRAS, M., TSUNG, F.S., MORI, W.B. & KATSOULEAS, T. 2006 A nonlinear theory for multidimensional relativistic plasma wave wakefields. *Phys. Plasmas* **13** (5), 056709.

MACCHI, A., CATTANI, F., LISEYKINA, T.V. & CORNOLTI, F. 2005 Laser acceleration of ion bunches at the front surface of overdense plasmas. *Phys. Rev. Lett*. **94** (16), 165003.

MACCHI, A., VEGHINI, S. & PEGORARO, F. 2009 'light sail' acceleration reexamined. *Phys. Rev. Lett*. **103** (8), 085003.

MAKSIMCHUK, A., GU, S., FLIPPO, K., UMSTADTER, D. & BYCHENKOV, V.Y. 2000 Forward ion acceleration in thin films driven by a high-intensity laser. *Phys. Rev. Lett*. **84** (18), 4108–4111.

PUKHOV, A. & MEYER TER VEHN, J. 2002 Laser wake field acceleration: the highly non-linear broken-wave regime. *Appl. Phys.* B*: Lasers Opt*. **74** (4-5), 355–361.

PUKHOV, A., SHENG, Z.-M. & MEYER TER VEHN, J. 1999 Particle acceleration in relativistic laser channels. *Phys. Plasmas* **6** (7), 2847–2854.

QIAO, B., ZEPF, M., BORGHESI, M. & GEISSLER, M. 2009 Stable GeV ion-beam acceleration from thin foils by circularly polarized laser pulses. *Phys. Rev. Lett.* **102** (14), 145002.

REMINGTON, B.A., DRAKE, R.P., TAKABE, H. & ARNETT, D. 2000 A review of astrophysics experiments on intense lasers. *Phys. Plasmas* **7** (5), 1641–1652.

ROBINSON, A.P.L., ZEPF, M., KAR, S., EVANS, R.G. & BELLEI, C. 2008 Radiation pressure acceleration of thin foils with circularly polarized laser pulses. *New J. Phys.* **10** (1), 013021.

ROSMEJ, O.N., GYRDYMOV, M., GÜNTHER, M.M., ANDREEV, N.E., TAVANA, P., NEUMAYER, P., ZÄHTER, S., ZAHN, N., POPOV, V.S., BORISENKO, N.G., *et al.* 2020 High-current laser-driven beams of relativistic electrons for high energy density research. *Plasma Phys. Control. Fusion* **62** (11), 115024.

ROTH, M., COWAN, T.E., KEY, M.H., HATCHETT, S.P., BROWN, C., FOUNTAIN, W., JOHNSON, J., PENNINGTON, D.M., SNAVELY, R.A., WILKS, S.C., *et al.* 2001 Fast ignition by intense laser-accelerated proton beams. *Phys. Rev. Lett.* **86** (3), 436–439.

SHEN, X.F., PUKHOV, A. & QIAO, B. 2021 Monoenergetic high-energy ion source via femtosecond laser interacting with a microtape. *Phys. Rev.* X **11** (4), 041002.

SHEN, X.F., QIAO, B., ZHANG, H., KAR, S., ZHOU, C.T., CHANG, H.X., BORGHESI, M. & HE, X.T. 2017 Achieving stable radiation pressure acceleration of heavy ions via successive electron replenishment from ionization of a high- z material coating. *Phys. Rev. Lett.* **118** (20), 204802.

SHIN, Y.-M. 2014 Beam-driven acceleration in ultra-dense plasma media. *Appl. Phys. Lett.* **105** (11), 114106.

SNAVELY, R.A., KEY, M.H., HATCHETT, S.P., COWAN, T.E., ROTH, M., PHILLIPS, T.W., STOYER, M.A., HENRY, E.A., SANGSTER, T.C., SINGH, M.S., *et al.* 2000 Intense high-energy proton beams from petawatt-laser irradiation of solids. *Phys. Rev. Lett.* **85** (14), 2945–2948.

TAJIMA, T. & DAWSON, J.M. 1979 Laser electron accelerator. *Phys. Rev. Lett.* **43** (4), 267–270.

WANG, X., ZGADZAJ, R., FAZEL, N., LI, Z., YI, S.A., ZHANG, X., HENDERSON, W., CHANG, Y.Y., KORZEKWA, R., TSAI, H.E., *et al.* 2013 Quasi-monoenergetic laser-plasma acceleration of electrons to 2 GeV. *Nat. Commun.* **4** (1), 1988.

WILKS, S.C., LANGDON, A.B., COWAN, T.E., ROTH, M., SINGH, M., HATCHETT, S., KEY, M.H., PENNINGTON, D., MACKINNON, A. & SNAVELY, R.A. 2001 Energetic proton generation in ultra-intense laser–solid interactions. *Phys. Plasmas* **8** (2), 542–549.

YAN, X.Q., LIN, C., SHENG, Z.M., GUO, Z.Y., LIU, B.C., LU, Y.R., FANG, J.X. & CHEN, J.E. 2008 Generating high-current monoenergetic proton beams by a circularly polarized laser pulse in the phase-stable acceleration regime. *Phys. Rev. Lett.* **100** (13), 135003.

YIN, L., ALBRIGHT, B.J., HEGELICH, B.M., BOWERS, K.J., FLIPPO, K.A., KWAN, T.J.T. & FERNÁNDEZ, J.C. 2007 Monoenergetic and GeV ion acceleration from the laser breakout after burner using ultrathin targets. *Phys. Plasmas* **14** (5), 056706.

YIN, L., ALBRIGHT, B.J., HEGELICH, B.M. & FERNÁNDEZ, J.C. 2006 GeV laser ion acceleration from ultrathin targets: the laser break-out after burner. *Laser Part. Beams* **24** (2), 291–298.

ZHANG, W.L., QIAO, B., HUANG, T.W., SHEN, X.F., YOU, W.Y., YAN, X.Q., WU, S.Z., ZHOU, C.T. & HE, X.T. 2016 Quasi-monoenergetic ion beam acceleration by laser-driven shock and solitary waves in near-critical plasmas. *Phys. Plasmas* **23** (7), 073118.